Supporting Information

A series of four-substituted polyoxometalate-thiacalix[4]arene-based materials for efficient photocatalytic reduction of Cr(VI) pollutant

Jia-Yi Zhang‡, Yuting Song‡, Jin Yang*, Wen-Yuan Pei and Jian-Fang Ma*

Key Laboratory of Polyoxometalate and Reticular Material Chemistry of Ministry of Education, Department of Chemistry, Northeast Normal University, Changchun 130024, China

*Corresponding author

E-mail: yangj808@nenu.edu.cn (J. Yang)

E-mail: majf247@nenu.edu.cn (J.-F. Ma)

‡These authors contributed equally to this manuscript.

I. Experimental Section

Characterization

Chemical reagents were purchased commercially. Fourier Transform Infrared (FT−IR) spectrum was determined on a Nicolet 6700 instrument. Thermogravimetric analysis (TGA) was carried out on a PerkinElmer TG−7 analyzer under N_2. Elemental analysis data was determined on a Euro Vector EA3000 elemental analyzer. Powder X−ray diffraction (PXRD) pattern was recorded on a Rigaku Dmax 2000 X−ray diffractometer with graphite monochromatized Cu Kα radiation (λ = 1.541 Å). UV−visible diffuse reflectance spectrum was measured on a UV−visible−near−IR spectrophotometer (Varian Cary 500). The absorbance spectrum of solution was determined on a Varian Cary 50 UV−visible spectrometer. Valence band X−ray photoelectron spectroscopy (VB−XPS) of **1**−**3** was determined on an ESCALAB250 with an Al Kα radiation. VB−XPS of **BWO** was determined on a FEI ESCALAB Xi+ with an Al Kα radiation. Photoluminescence (PL) spectra were analyzed with fluorescence spectrometry (Hitachi F−4600). ^{1}H NMR data was measured on a Bruker 500 MHz instrument. Nitrogen adsorption-desorption experiment was conducted on an Autosorb-iQ instrument.

X−ray Crystallography

Single crystal X−ray data for **1** and **2** were collected on a Bruker APEXII X−ray diffractometer equipped with a CMOSPHOTON 100 detector with a Mo Kα X−ray source (λ = 0.71073 Å) at 170 K. Single−crystal X−ray diffraction data for **3** was collected on an Oxford diffraction Gemini R Ultra diffractometer with graphite

monochromated Mo K_α radiation (λ = 0.71073 Å) at 298 K. The structures of **1**−**3** were solved by direct method and refined by the full−matrix least−squares method on F^2 values using the SHELXL 2018/3.[1–3] Non−H atoms were refined with anisotropic parameters. Some atoms in **1**−**3** were split over two parts with the total occupancy of 1. The formula of **1**−**3** was established by electron diffraction density, thermogravimetric analysis and elemental analysis. CCDC numbers are 2303754, 2303755 and 2303756.

Synthesis of $[Mn_2L_2(H_2O)_2][H_3Mn_4PW_{10}O_{40}]\cdot 2C_2H_5OH\cdot 4H_2O$ (1)

A mixture of **L** (10 mg, 0.0075 mmol), $MnCl_2\cdot 4H_2O$ (7 mg, 0.03 mmol), $H_3PW_{12}O_{40}\cdot xH_2O$ (18 mg, 0.011 mmol), NaOH solution (80 μL, 0.2 M) and H_2O/EtOH (8 mL, 2/6, v/v) was heated in an autoclave at 100 °C for 72 hours. After cooling to room temperature, yellow crystals of **1** were obtained (yield: 51%). Anal. Calcd. for $C_{140}H_{179}Mn_6N_8O_{64}PS_{16}W_{10}$ (*Mr* = 5709.97): C, 29.45; N, 1.96; S, 8.99. Found: C, 29.38; N, 1.87; S, 8.81. IR (KBr, cm^{-1}) : 3435 (m), 2957 (w), 2866 (w), 1621 (w), 1560 (w),1471 (m), 1429 (w), 1378 (w), 1260 (w), 1212 (w), 1151 (w), 1080 (s), 979 (s), 896 (m), 819 (s), 754 (w), 700 (w), 510 (w).

Synthesis of $[Cd_2L_2(H_2O)_2][H_3Cd_4PW_{10}O_{40}]\cdot C_2H_5OH\cdot 3H_2O$ (2)

A mixture of **L** (10 mg, 0.0075 mmol), $CdCl_2$ (9 mg, 0.05 mmol), $H_3PW_{12}O_{40}\cdot xH_2O$ (18 mg, 0.011 mmol), NaOH solution (90 μL, 0.2 M) and H_2O/EtOH (8 mL, 2/6, v/v) was heated in an autoclave at 100 °C for 72 hours. Colorless crystals of **2** were obtained (yield: 46%) after cooling to room temperature. Anal. Calcd. for $C_{138}H_{171}Cd_6N_8O_{62}PS_{16}W_{10}$ (*Mr* = 5990.65): C, 27.67; N, 1.87; S, 8.56. Found: C,

27.48; N, 1.73; S, 8.43. IR (KBr, cm^{-1}) : 3436 (m), 2961 (w), 2866 (w), 1621 (w), 1563 (w), 1470 (w), 1427 (w), 1378 (w), 1266 (w), 1213 (w), 1145 (w), 1080 (m), 978 (m), 896 (m), 819 (s), 754 (w), 703 (w), 518 (w).

Synthesis of $[Ni_2L_2(H_2O)_2][H_3Ni_4PW_{10}O_{40}]\cdot 2C_2H_5OH\cdot 5H_2O$ (3)

A mixture of **L** (10 mg, 0.0075 mmol), $NiCl_2\cdot 4H_2O$ (7 mg, 0.03 mmol), $H_3PW_{12}O_{40}\cdot xH_2O$ (18 mg, 0.011 mmol), NaOH solution (120 μL, 0.2 M) and H_2O/EtOH (8 mL, 2/6, v/v) was heated in an autoclave at 100 °C for 72 hours. Yellow crystals of **3** were gained (yield: 43%) after cooling to room temperature. Anal. Calcd. for $C_{140}H_{181}Ni_6N_8O_{65}PS_{16}W_{10}$ (*Mr* = 5750.61): C, 29.24; N, 1.95; S, 8.92. Found: C, 29.52; N, 1.92; S, 8.89. IR (KBr, cm^{-1}) : 3434 (m), 2960 (w), 2870 (w), 1625 (w), 1570 (w), 1471 (m), 1427 (m), 1379 (w), 1267 (w), 1210 (w), 1149 (w), 1080 (s), 978 (s), 896 (s), 819 (s), 755 (w), 704 (w), 522 (w).

Synthesis of Bi_2WO_6

Bi_2WO_6 (**BWO**) was synthesized by the literature method.[4] A mixture of $Bi(NO_3)_3\cdot 5H_2O$ (4.85 g, 10 mmol), $Na_2WO_4\cdot 2H_2O$ (1.65 g, 5 mmol) and 50 mL distilled water was stirred for 1 h and heated in an autoclave at 140 °C for 20 h. The resulting white solid sample was filtrated, washed three times with deionized water and ethanol, respectively, and dried at 60 °C overnight. The BWO microspheres was obtained after calcining at 300 °C for 4 h (yield 65%).

Synthesis of BWO/1

A certain amount of **BWO** and **1** were ground in an agate grinder for 20 minutes to obtain a series of **BWO**/**1** composite materials. In this experiment, the mass of **1** was

constant at 20 mg. The **BWO/1** composite materials with mass ratios (**BWO**:**1**) of 0.20:1, 0.40:1, 0.60:1, 0.80:1, 1:1, referred to as 20**BWO/1**, 40**BWO/1**, 60**BWO/1**, 80**BWO/1** and 100**BWO/1**, were prepared by varying the amount of **BWO**.

Electrochemical experiments

Electrochemical test was performed on an electrochemical workstation (CHI 760E, Shanghai Chenhua). A typical three−electrode system was used at room temperature with a Pt electrode as the counter electrode, and a saturated calomel electrode (SCE) as the reference electrode. A 300 W Xenon lamp (PLS−SXE300) was employed as the light source, and 0.5 M Na_2SO_4 aqueous solution was used as the electrolyte. The transient photocurrent response test was performed at 0.6 V (*vs.* SCE). Electrochemical impedance spectroscopy (EIS) was determined from 0.1 to 10^6 Hz at 0 V (*vs.* SCE). The Mott−Schottky curve of **BWO** and **1**−**3** was achieved at 1000, 1500, 2000 and 2500 Hz without light. For the preparation of the working electrode, the sample (5 mg for **1**−**3**, 4 mg for **BWO** and 9 mg for 80**BWO/1**) was dispersed in 180 μL ethanol solution and 20 μL Nafion solution (5 wt%), and sonicated for 30 min at room temperature. Subsequently, the suspension was evenly dropped on a fluorine−doped tin oxide (FTO) glass with an area of 1 cm^2.

Photocatalytic reduction of Cr(VI) with 1−3 as photocatalyst

Photocatalytic efficiencies of **1**−**3** for the reduction from Cr(VI) to Cr(III) were evaluated under the UV light. In the photocatalytic reduction experiments, 40 mL Cr(VI) solution was added to the quartz reactor. The pH value was adjusted by adding an appropriate amount of 0.1 M H_2SO_4 and NaOH. After stirring for 30 min in the

dark, the adsorption−desorption equilibrium was achieved. Then the light was turned on and 1 mL solution was taken and filtered every 20 min. The Cr(VI) concentration was tested by the diphenylcarbazide method.[5] The solution absorbance spectrum was measured with a UV−visible spectrometer, and the maximum absorption wavelength was determined at 542 nm, which was used to judge the residual Cr(VI) content in the filtrate. According to Eq. (1), the reduction rate of Cr(VI) was calculated. C and C_0 represent the concentrations of Cr(VI) at t and 0 min, respectively.

$$\text{Reduction rate} = \frac{C_0 - C}{C} \times 100\% \qquad (1)$$

Photocatalytic reduction of Cr(VI) with BWO/1 as photocatalyst

The photocatalytic performances for the reduction of Cr(VI) of **BWO/1** and **BWO** were evaluated under the UV light. Typically, the catalyst was added into a 40 mL solution with the Cr(VI) concentration of 15 mg/L, which was prepared by dissolving dried $K_2Cr_2O_7$ in deionized water. The solution pH was adjusted to 2 with 0.1 M H_2SO_4 solution. Prior to illumination, the reaction solutions were stirred for 30 min in the dark to reach adsorption−desorption equilibrium. Then 1 mL solution was taken and filtered every 20 min. The concentrations of Cr(VI) were recorded by the diphenylcarbazide method.[5] The reduction rate of Cr(VI) was calculated by Eq. (1). The Cr(VI) content was determined with a UV−visible spectrometer at 542 nm.

II. Supporting Figures

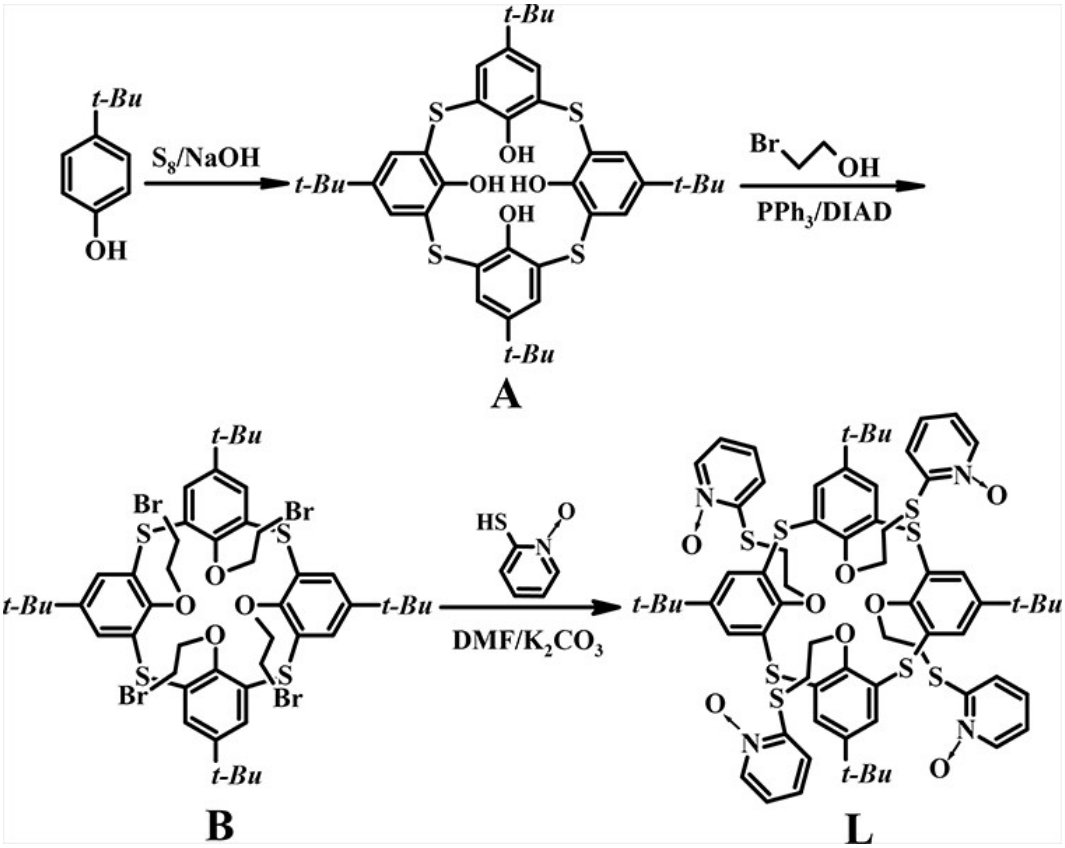

Scheme S1. Synthetic route for **L**.

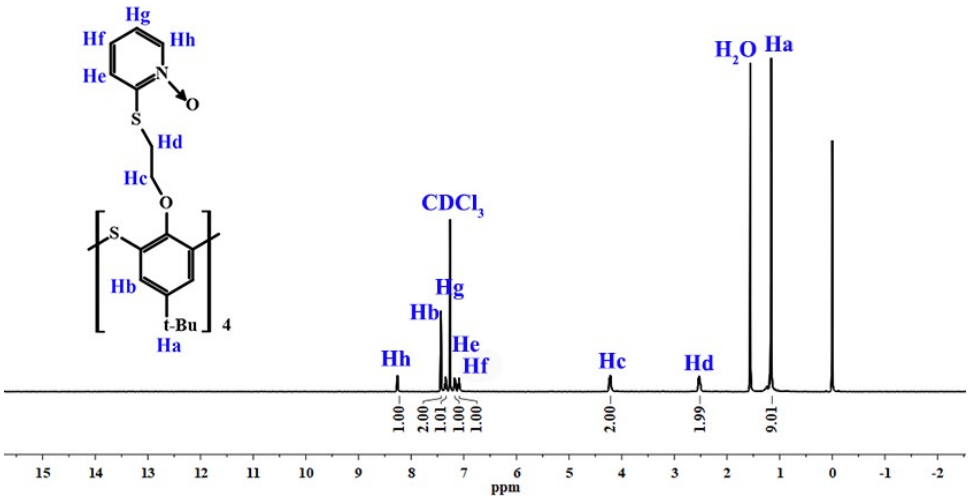

Fig. **S1**. ^{1}H NMR spectrum of **L**.

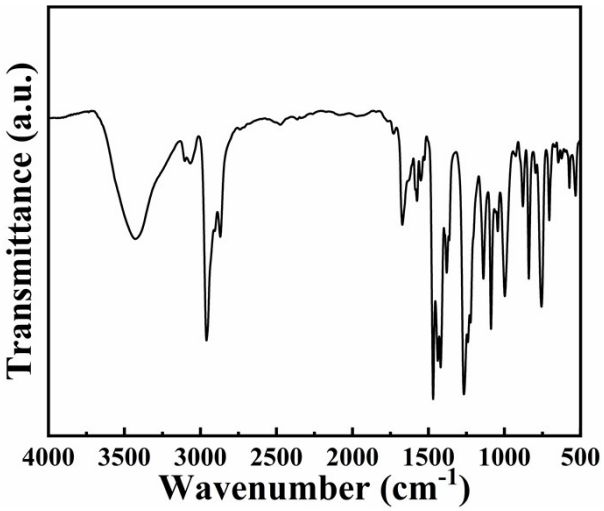

Fig. **S2**. FT−IR spectrum of **L**.

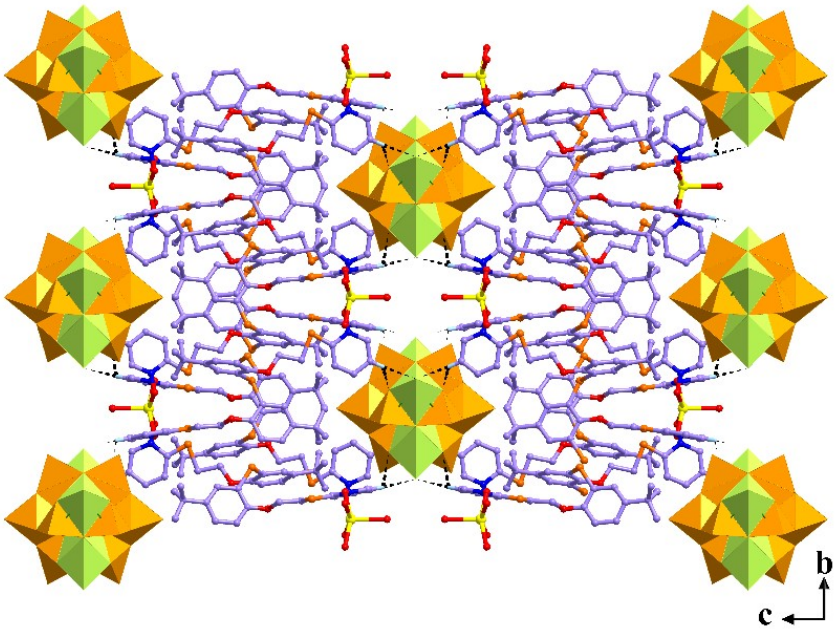

Fig. **S3**. 3D supramolecular architecture formed by hydrogen bonds in **1**.

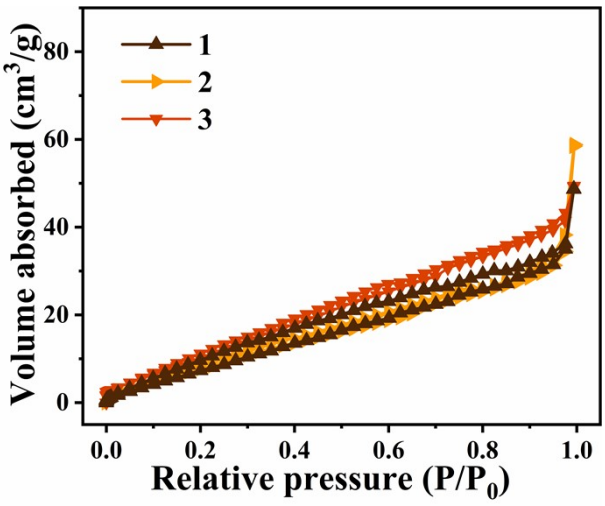

Fig. S4. N_2 adsorption–desorption isotherms of **1**−**3**.

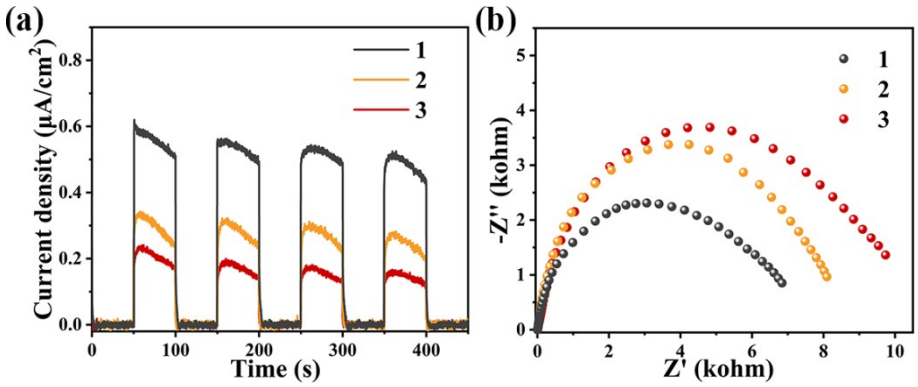

Fig. S5. (a) Photocurrent response curves of **1**−**3**. (b) EIS Nyquist plots of **1**−**3**.

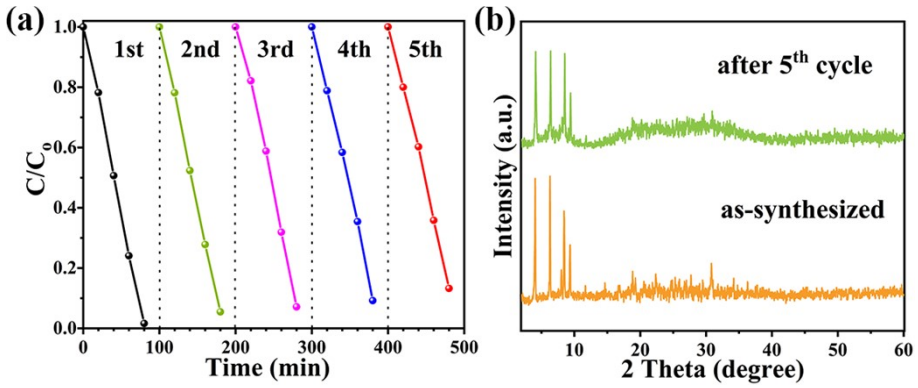

Fig. S6. (a) Reusability tests of **1**. (b) PXRD patterns of **1** before and after the reusability tests.

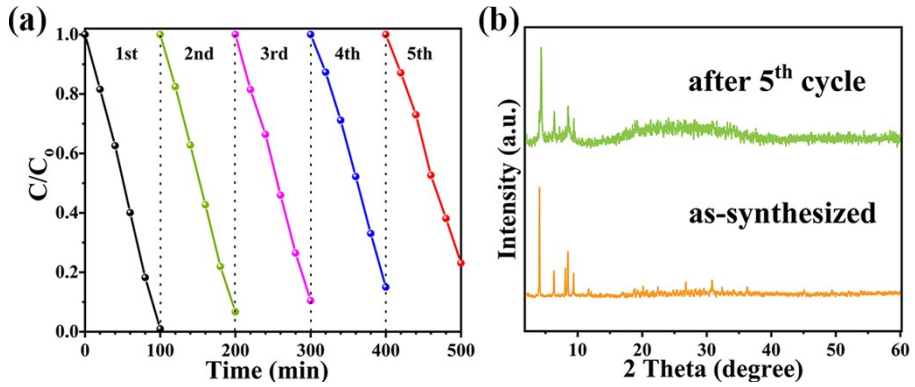

Fig. **S7**. (a) Reusability tests of **2**. (b) PXRD patterns of **2** before and after the reusability tests.

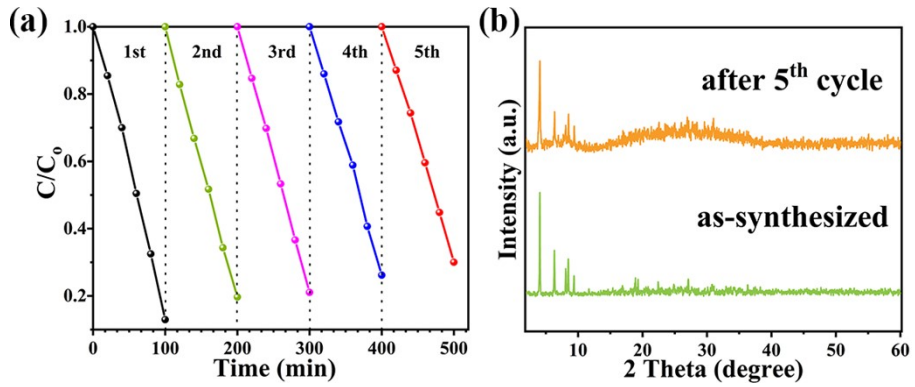

Fig. **S8**. (a) Reusability tests of **3**. (b) PXRD patterns of **3** before and after the reusability tests.

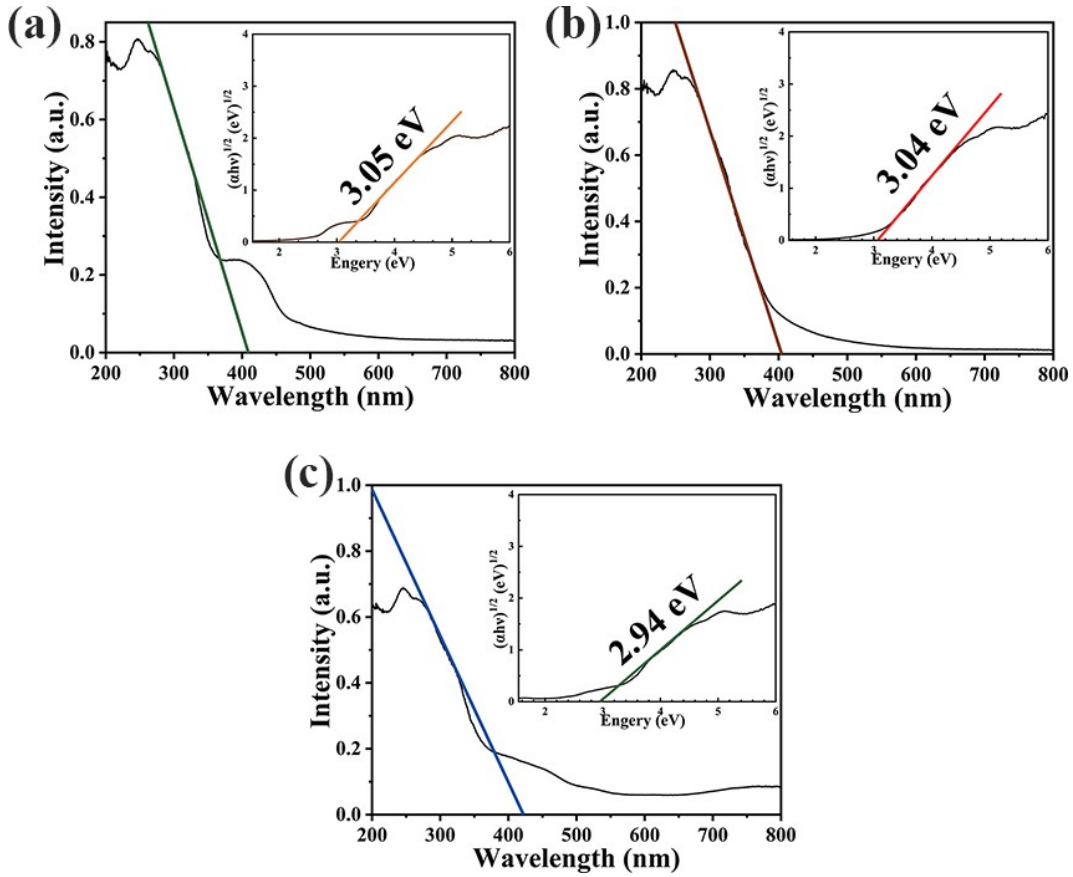

Fig. **S9**. UV−vis DRS and Tauc plots of **1** (a), **2** (b), and **3** (c).

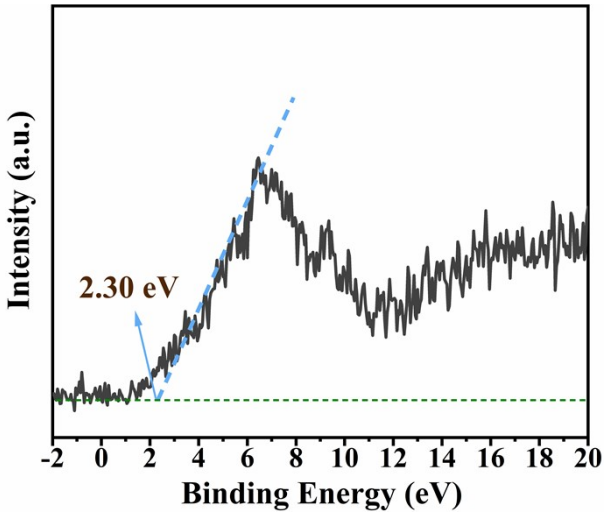

Fig. **S10**. VB−XPS spectrum of **1**.

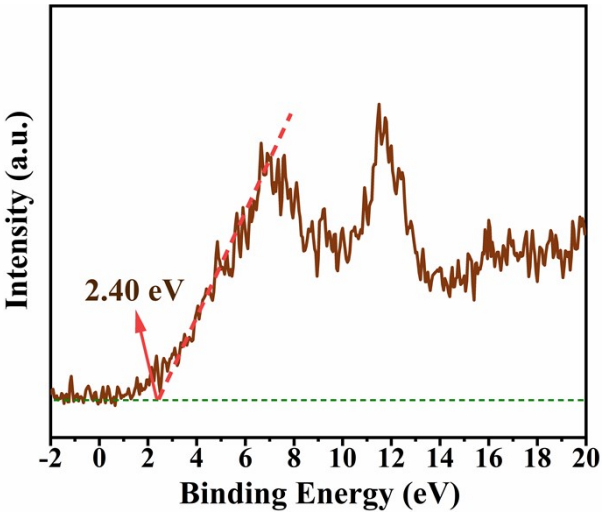

Fig. S11. VB−XPS spectrum of **2**.

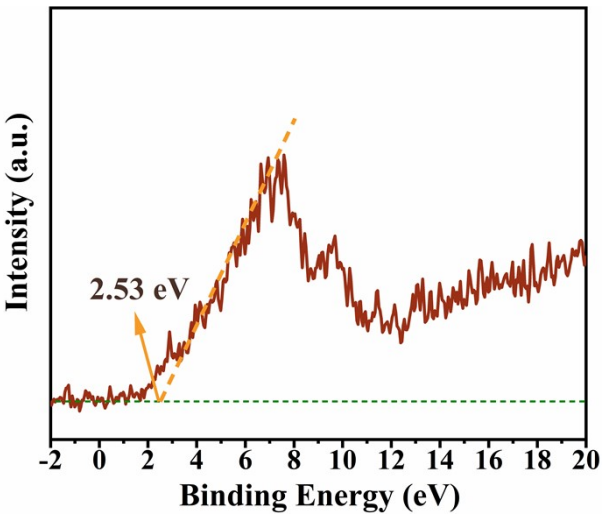

Fig. S12. VB−XPS spectrum of **3**.

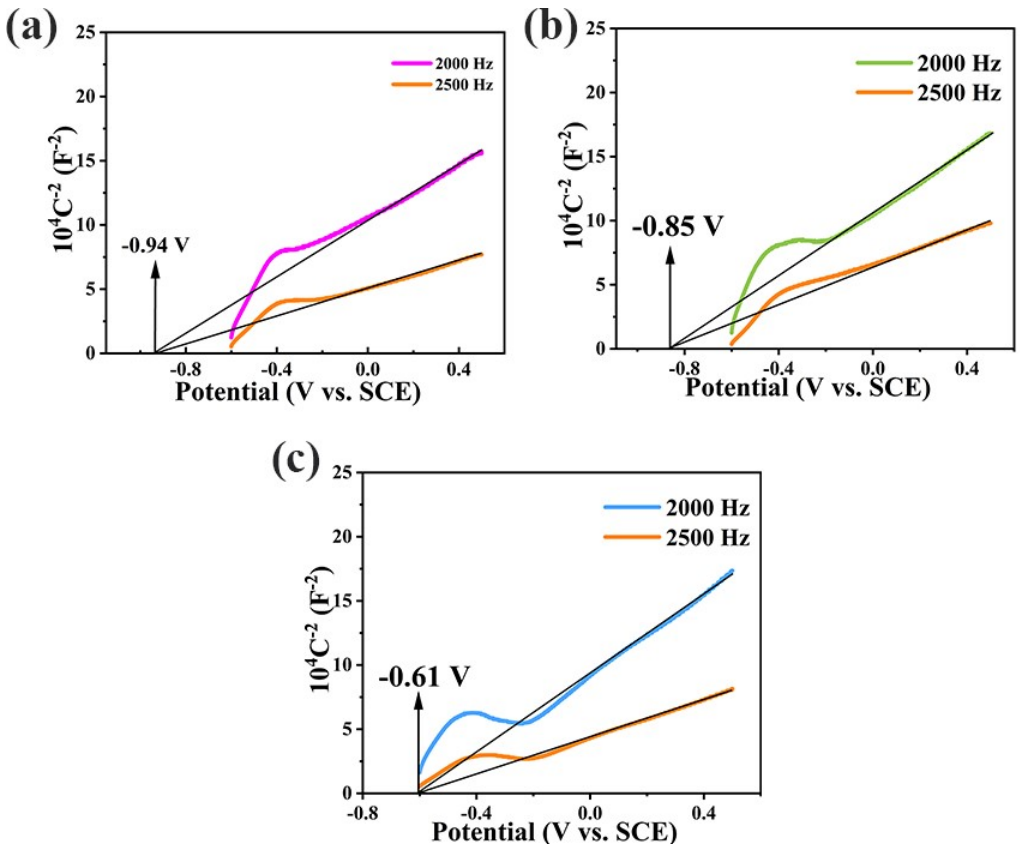

Fig. **S13**. Mott–Schottky curves of **1** (a), **2** (b) and **3** (c).

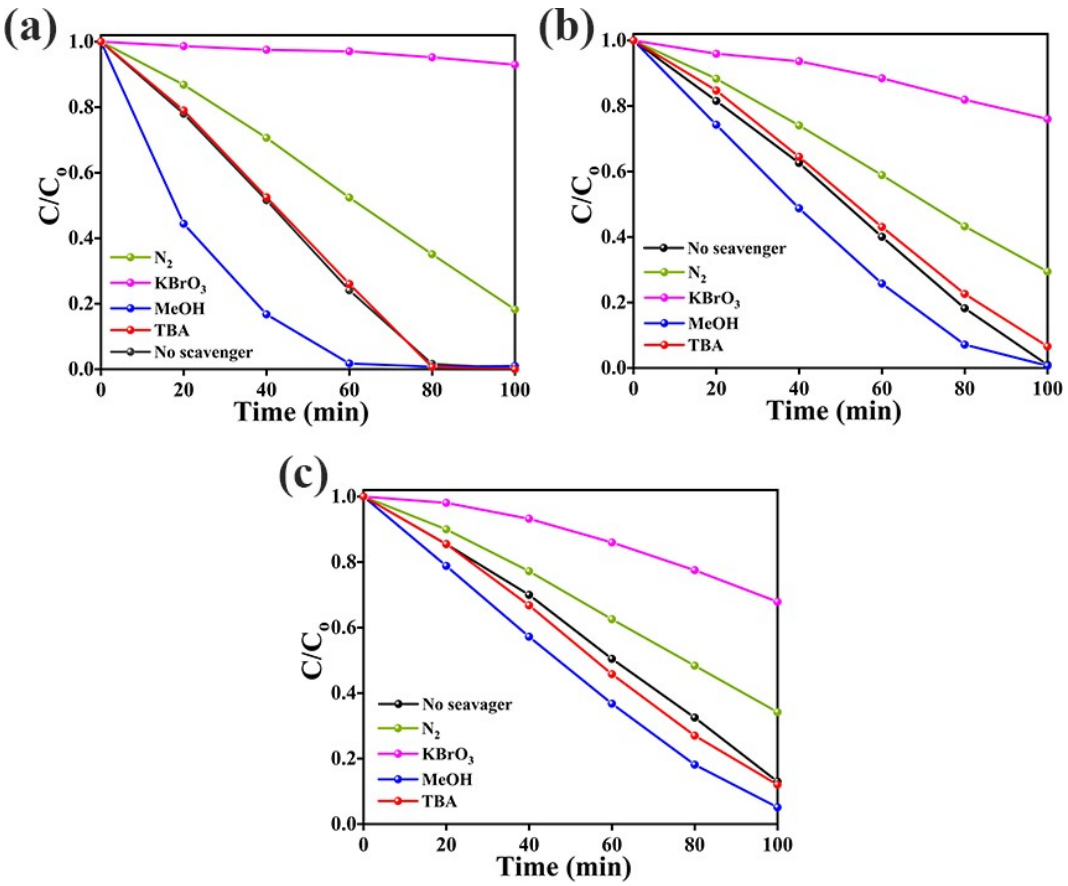

Fig. **S14**. Trapping experiments for the photocatalytic activities of **1** (a), **2** (b) and **3** (c) with different scavengers.

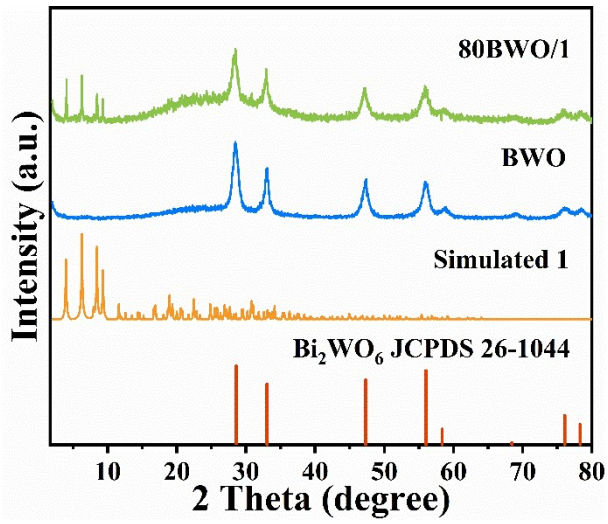

Fig. **S15**. PXRD patterns of **BWO** and 80**BWO**/**1**.

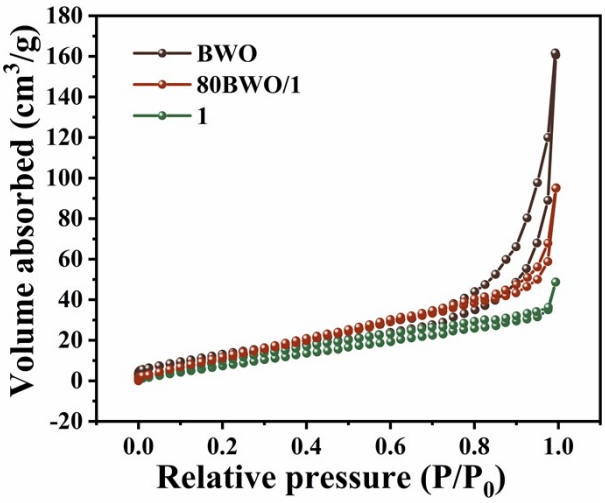

Fig. **S16**. N_2 adsorption–desorption isotherms of **BWO**, 80**BWO/1** and **1**.

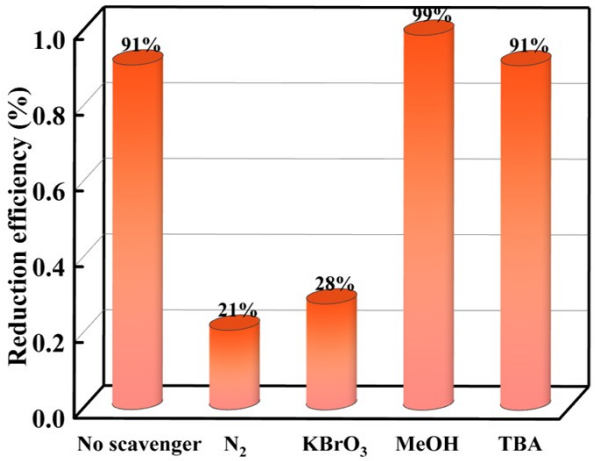

Fig. **S17**. Trapping experiments for the photocatalytic activities of 80**BWO/1** with different scavengers.

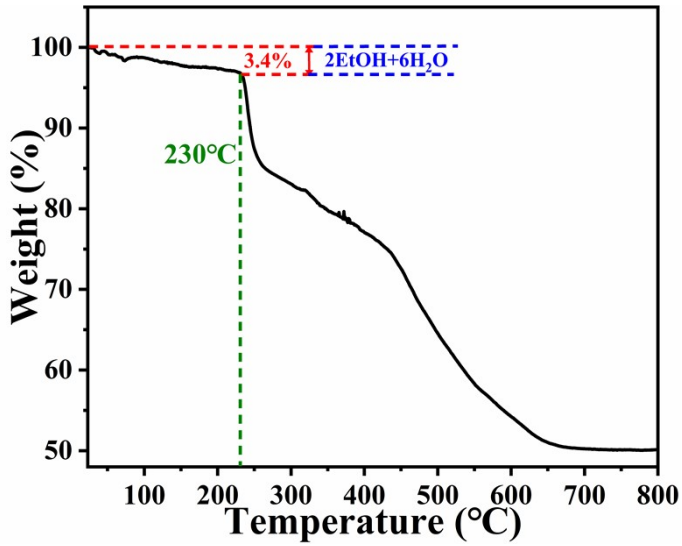

Fig. **S18**. TGA curve of **1**.

The weight loss of **1** before 230 ℃ corresponded to the removal of two coordination water molecules, four free water molecules and two free ethanol molecules (obsd. 3.4%, calcd. 3.48%).

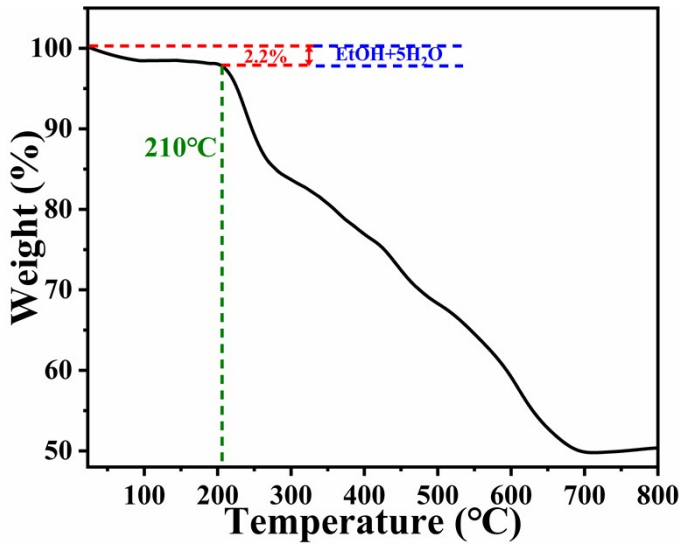

Fig. **S19**. TGA curve of **2**.

The weight loss before 210 ℃ was ascribed to the removal of two coordination water molecules, three free water molecules and one free ethanol molecule (obsd. 2.2%, calcd. 2.27%).

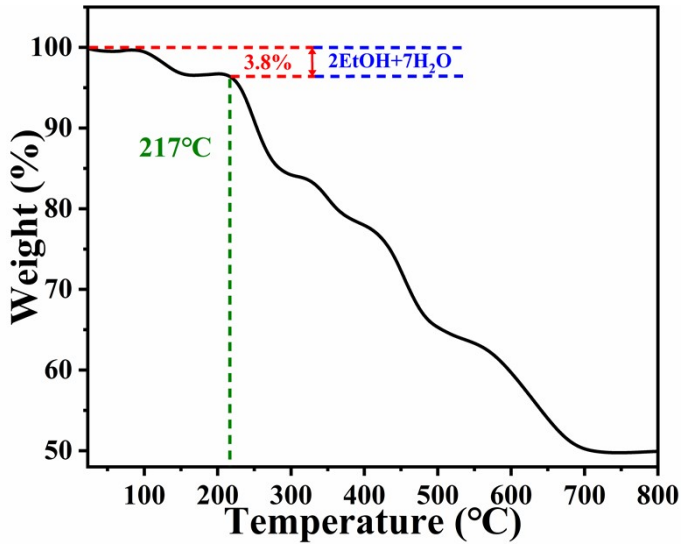

Fig. **S20**. TGA curve of **3**.

The weight loss of 3.8% before 217 ℃ was assigned to the loss of two coordination water molecules, five free water molecules and two free ethanol molecules (calcd. 3.79%).

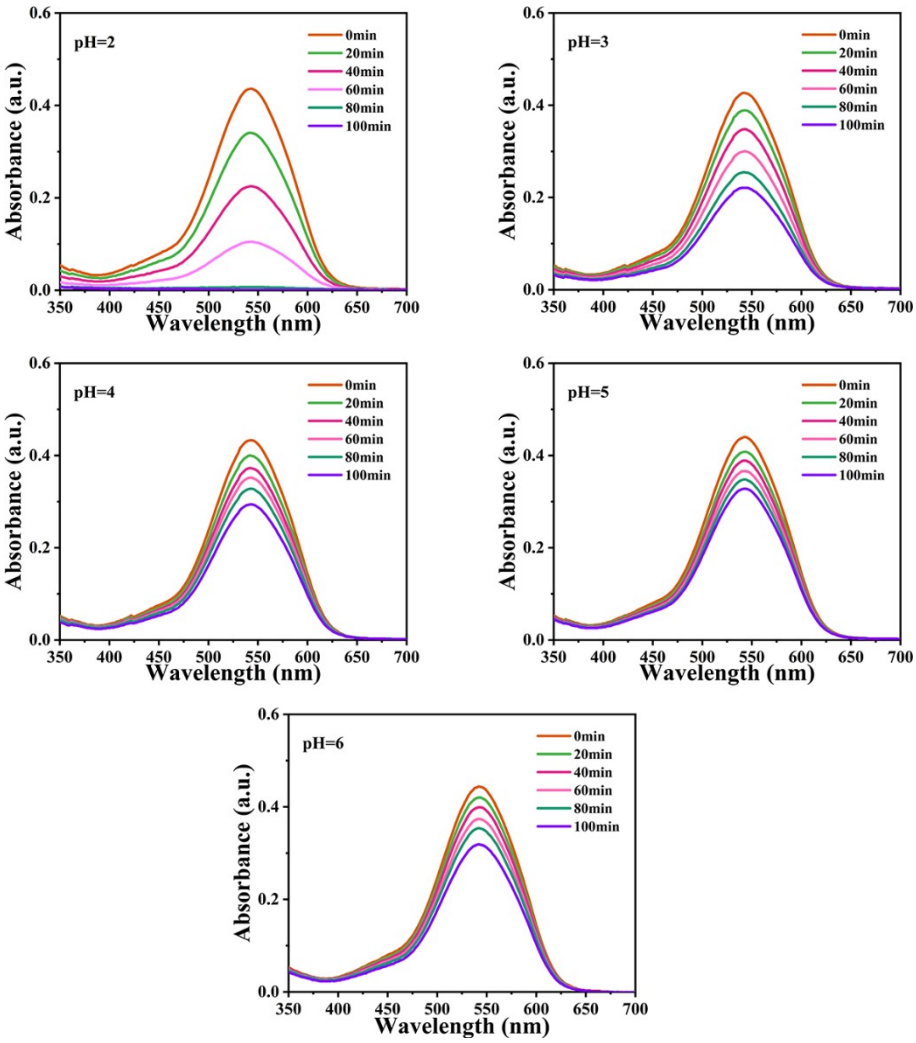

Fig. **S21**. UV−visible absorption spectra of Cr(VI) aqueous solution at different pH values by **1** photocatalysis.

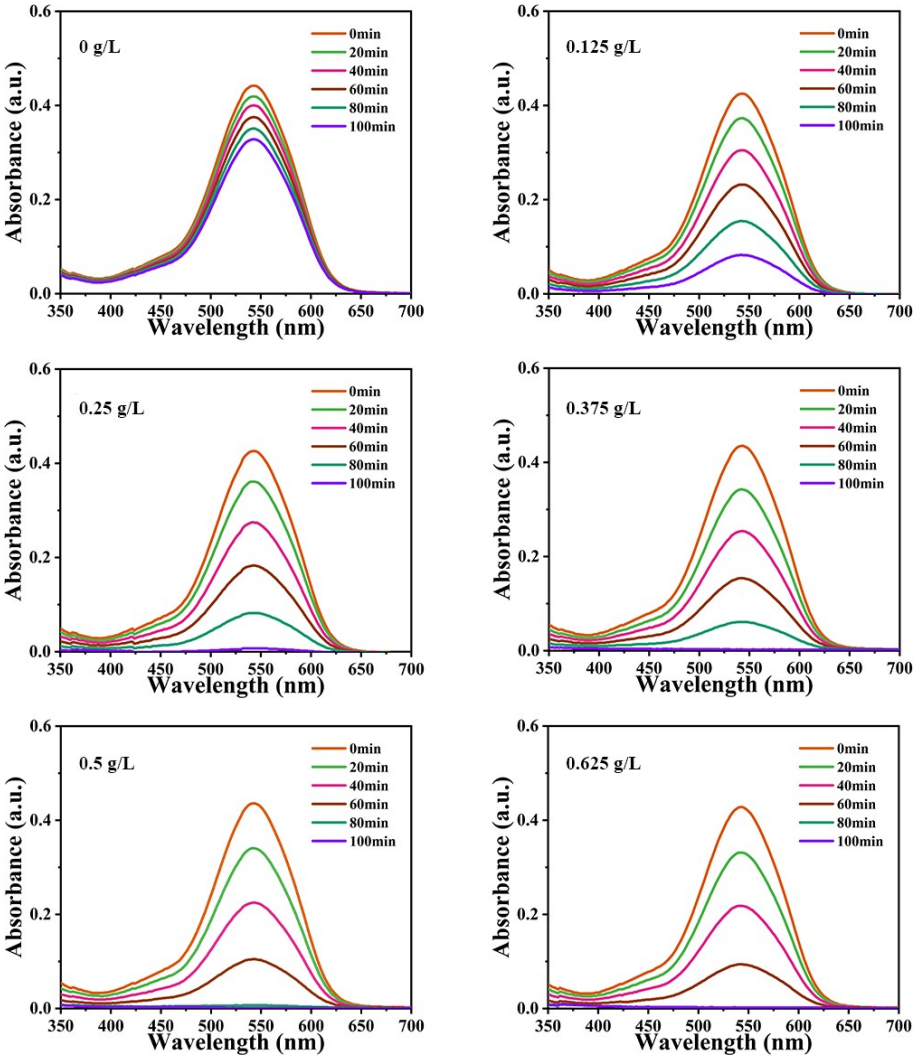

Fig. **S22**. UV−visible absorption spectra of Cr(VI) aqueous solution with different amounts of **1**.

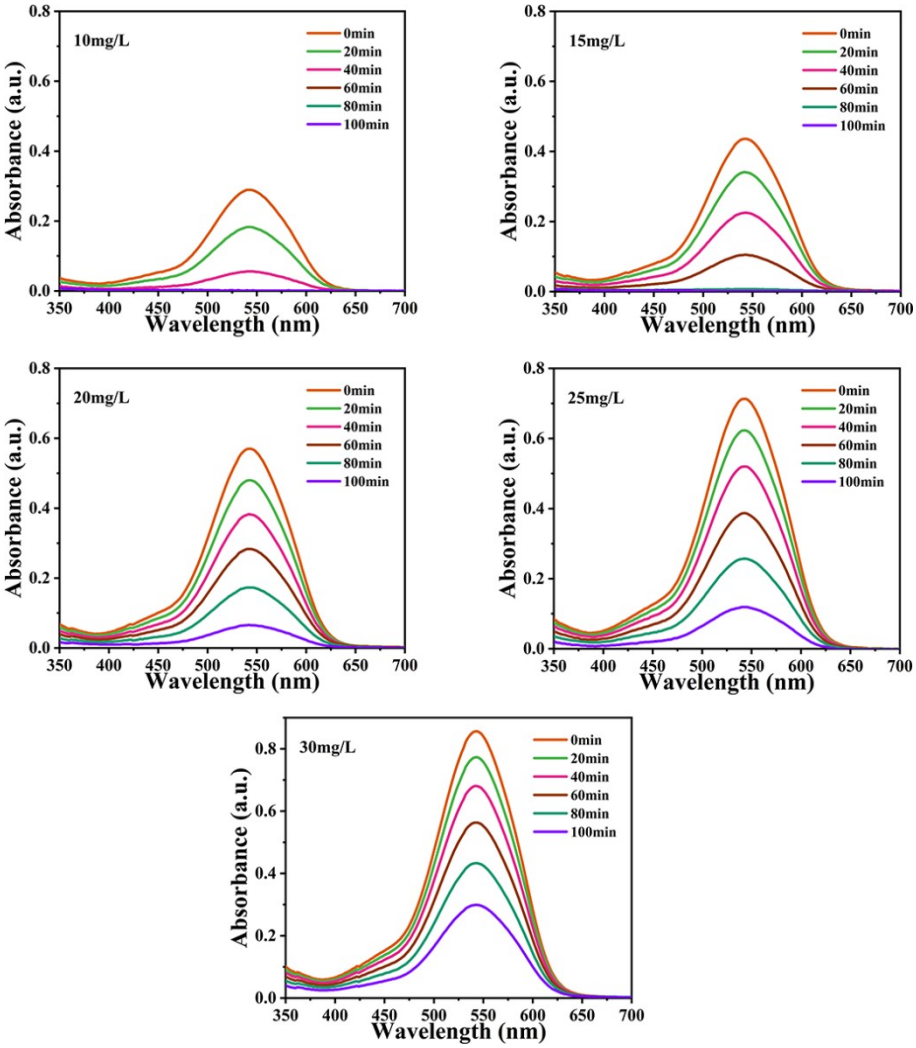

Fig. **S23**. UV−visible absorption spectra of Cr(VI) aqueous solution with different substrate concentrations by **1** photocatalysis.

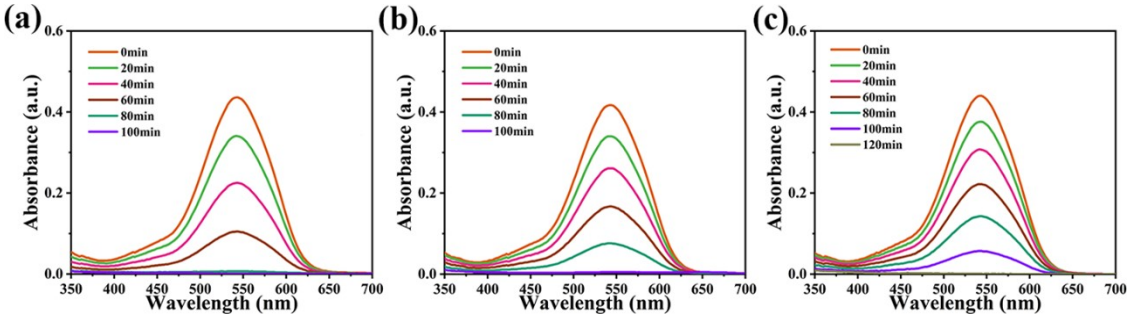

Fig. **S24**. UV−visible absorption spectra of Cr(VI) aqueous solution with **1** (a), **2** (b), **3** (c) as photocatalyst.

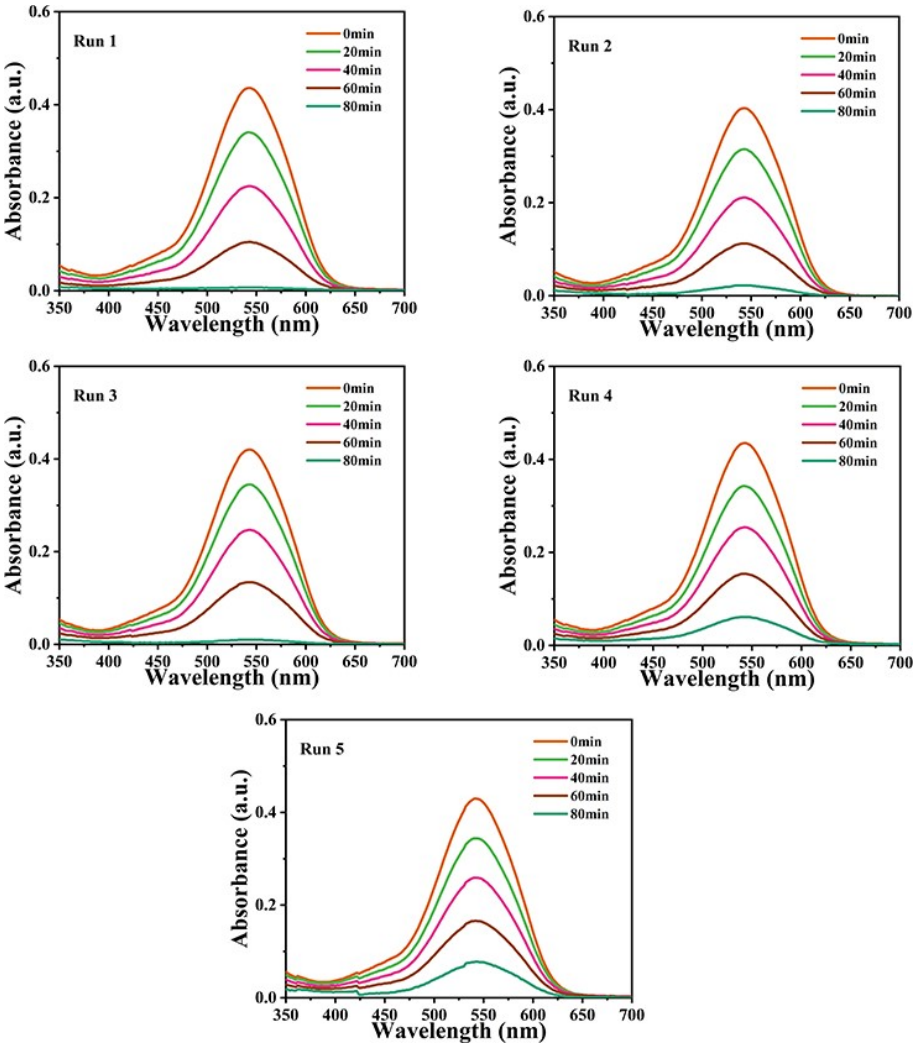

Fig. **S25**. UV−visible absorption spectra of the reusability test with **1** as photocatalyst.

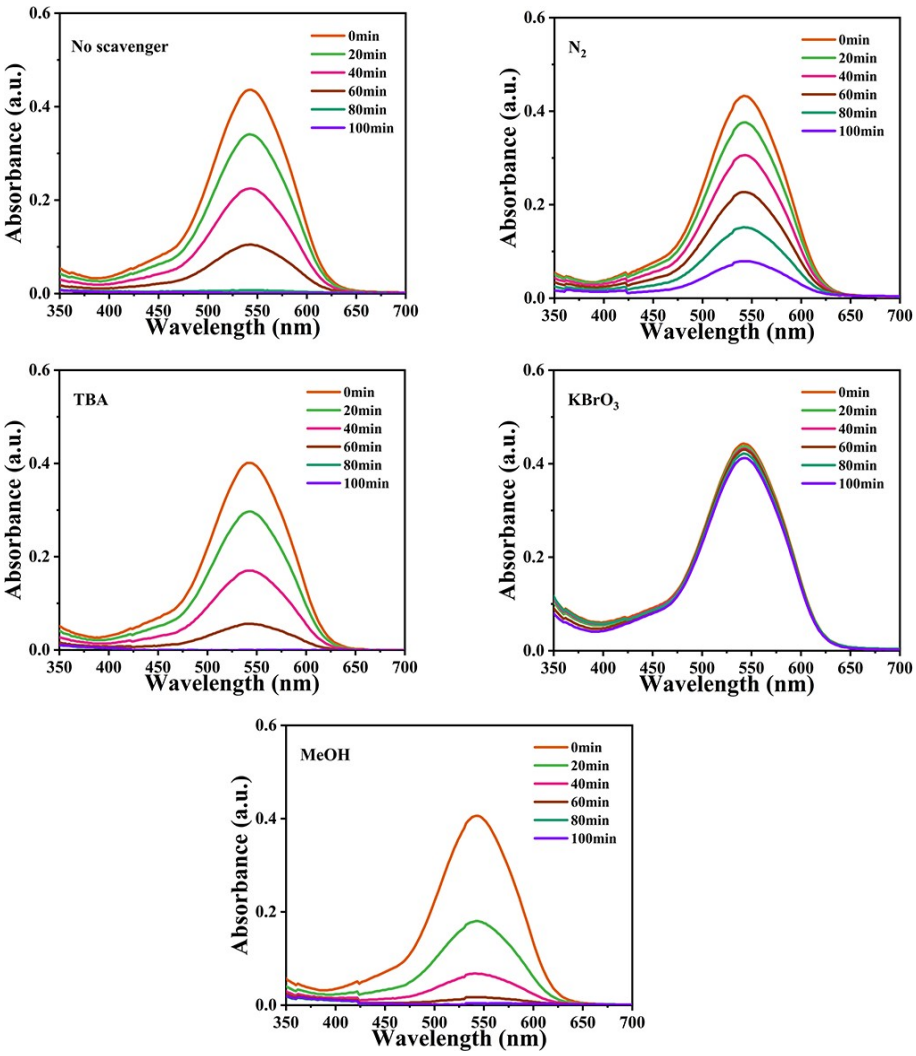

Fig. **S26**. UV−visible absorption spectra of Cr(VI) aqueous solution after adding different scavengers with **1** as photocatalyst.

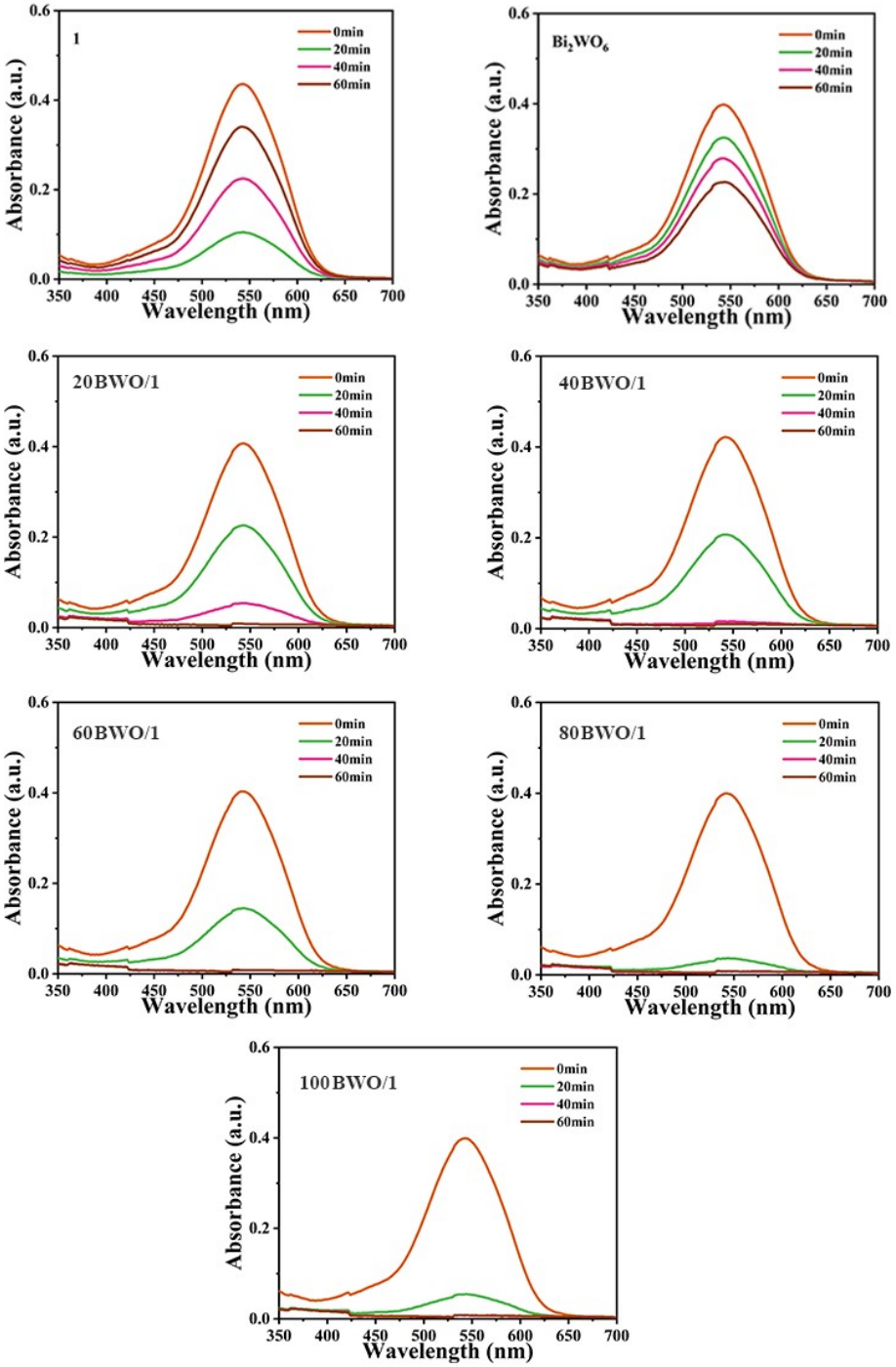

Fig. **S27**. UV−visible absorption spectra of Cr(VI) aqueous solution with **1**, **BWO** and **BWO/1** as photocatalyst.

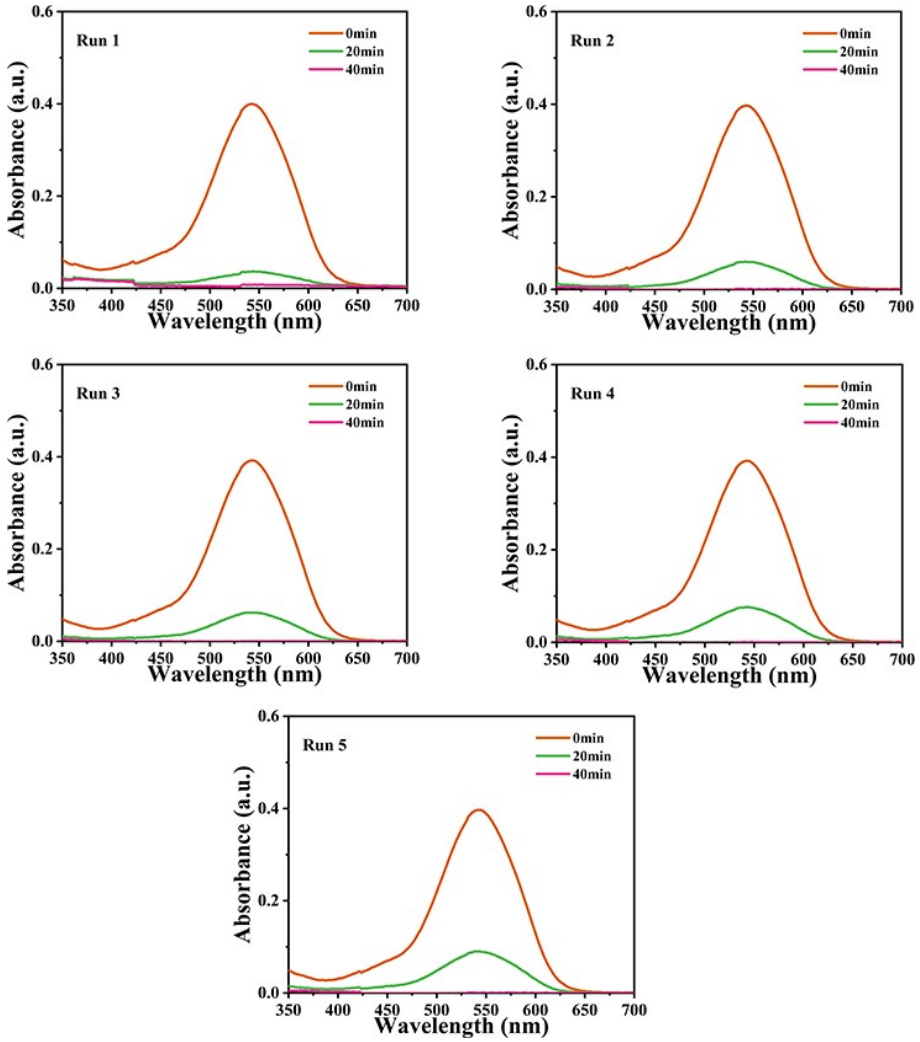

Fig. **S28**. UV−visible absorption spectra of the reusability test with 80**BWO**/**1** as photocatalyst.

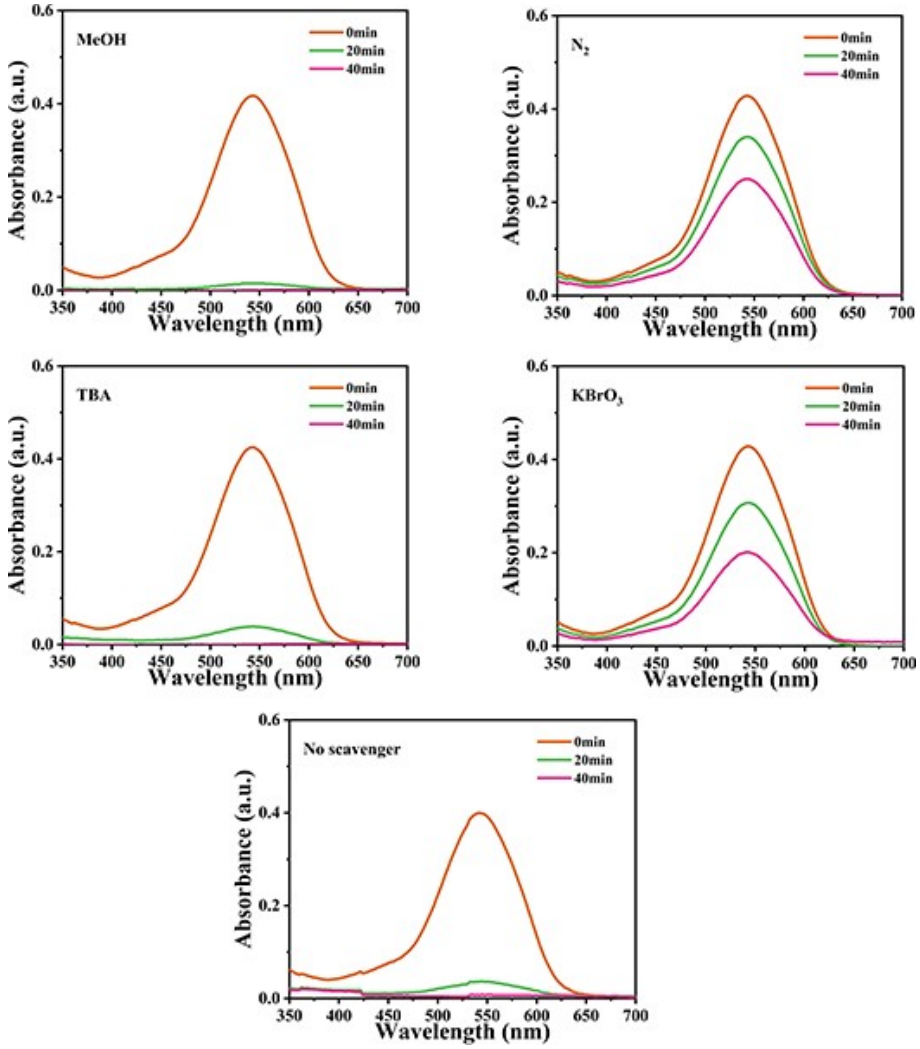

Fig. **S29**. UV−visible absorption spectra of Cr(VI) aqueous solution with 80**BWO**/**1** as photocatalyst after adding different scavengers.

Table S1. Comparison of Cr(VI) reduction rates with different photocatalysts.

Photocatalyst/ Dosage (mg)	Reaction solution volume (mL) / Concentration (mg/L) / pH	Scavenger/ Amount (mmol)	Light source	Illumination time (min)	Reduction rate (%)	Refs.
MoS_2−PVP/20	20/30/2.6	−	visible light	120	99.5	6
MIL−125(Ti)/50	50/10/2	TA/1	UV light	120	99.4	7
Ag/TiO_2/$CoFe_2O_4$/5	50/5/2	−	UV light	150	95.1	8
c−SB/TiO_2/25	50/10/2	−	UV light	180	98.56	9
$CuNb_2O_6$/g−C_3N_4/20	100/20/3	−	visible light	150	92.8	10

SnO_2/g−C_3N_4/diatomite/100	100/20/3	CA/0.5	visible light	150	98.6	11
Co−doped V_2O_5/30	−/20/7	−	simulated sunlight	100	90.5	12
$LaFeO_3$/g−C_3N_4/30	50/10/−	$Na_2C_2O_4$/1	full light	120	>90	13
Ag@NH_2−MIL−88B(Fe)/10	100/23.5/5	AO/0.021	LED lamp	80	99.99	14
$Ti_{0.4}$−$Zn_{0.6}$−UiO−66−NH_2/5	50/20/2	−	full light	120	99.8	15
CdS/g−C_3N_4/50	50/10/−	−	full light	60	64	16
20Fe−O@ZIF−L/50	100/30/7	CA/0.2	full light	90	86.6	17
CdTe/30	50/50/7	−	full light	180	82.44	18
Ta_3N_5/BiOCl/30	100/20/2.5	−	visible light	80	91.6	19
CeO_2/$CaIn_2S_4$/50	50/50/5.6	−	visible light	105	95	20
Tb@Zr−MOF/10	30/31/−	FA/530.4	UV light	60	97.5	21
Zn−MOF/40	40/20/2	EtOH/17.2	Sunlight	90	93	22
Cd−MOF/7	40/10/3	MeOH/0.005	UV light	50	100	23
1/20	40/15/2	−	UV light	80	97.6	This work
2/20	40/15/2	−	UV light	100	99.9	This work
3/20	40/15/2	−	UV light	120	99.9	This work

TA = tartaric acid, CA = citric acid, AO = ammonium oxalate monohydrate, and FA = formic acid.

Table S2. Comparison of Cr(VI) reduction rates with different composite **BWO** materials .

Photocatalyst/ Dosage (mg)	Reaction solution volume (mL)/ Concentration (mg/L)	Light source	Irradiation time (min)	Reduction efficiency (%)	Refs.
FeC_2O_4/**BWO**/50	50/20	565 mW cm^{-2} light	30	100	24
Ti_3C_2/**BWO**/75	50/10	visible light	120	92.5	25

PW_{12}/CN@**BWO**/30	50/20	1 kW Xe lamp	90	98.7	26
CeO_2@**BWO**/20	40/8	300W Xe lamp	60	99.6	27
$S_{0.10}$F-**BWO**/50	50/50	300 W Xe lamp	120	94.3	28
$MgIn_2S_4$/**BWO**/50	100/35	300 W Xe lamp	40	100	29
C_3N_5/**BWO**/20	100/10	300 W Xe lamp	50	97	30
BWO/$ZnIn_2S_4$/50	50/50	250 W Xe lamp	90	97.36	31
TaON/**BWO**/20	100/10	300 W Xe lamp	50	95.6	32
80**BWO**/**1**/36	15/40	UV lamp	20	91	This work

Table S3. Crystallographic data for **1**–**3**.

	1	**2**	**3**
Formula	$C_{140}H_{179}Mn_6N_8O_{64}PS_{16}W_{10}$	$C_{138}H_{171}Cd_6N_8O_{62}PS_{16}W_{10}$	$C_{140}H_{181}N_8Ni_6O_{65}PS_{16}W_{10}$
Mr	5709.97	5990.65	5750.61
Crystal system	tetragonal	tetragonal	tetragonal
Space group	*I*4/*m*	*I*4/*m*	*I*4/*m*
a (Å)	14.816(3)	14.8942(14)	14.9033(5)
c (Å)	44.354(10)	44.431(6)	44.2544(17)
V (Å^3)	9736(5)	9856(2)	9829.3(8)
Z	2	2	2
D_{calc} [g·cm^{-3}]	1.948	2.019	1.942
F(000)	5490.0	5700	5546.0
R_{int}	0.0840	0.1335	0.0867
GOF on F^2	1.015	0.921	1.042
R_1[a] *[I>2σ(I)]*	0.1058	0.0981	0.0950
wR_2[b] (all data)	0.2950	0.2657	0.2944

[a] $R_1 = \Sigma||F_o|-|F_c||/\Sigma|F_o|$. [b] $wR_2 = \{\Sigma[w(F_o^2-F_c^2)^2]/\Sigma w(F_o^2)^2]\}^{1/2}$

Table S4. Selected bond lengths (Å) and angles (°) for compound **1**.

1			
Mn(1)-O(1)	2.056(17)	Mn(2)-O(6)$^{\#4}$	1.8253(7)
Mn(1)-O(1)$^{\#2}$	2.056(17)	Mn(2)-O(6)$^{\#1}$	1.8253(7)
Mn(1)-O(1)$^{\#1}$	2.056(17)	Mn(2)-O(7A)	1.829(10)
Mn(1)-O(1)$^{\#3}$	2.056(17)	Mn(2)-O(8)	1.641(13)
Mn(1)-O(1W)	2.36(2)	Mn(2)-O(7B)	1.836(19)
O(1)-Mn(1)-O(1)$^{\#2}$	87.91(17)	O(6)$^{\#1}$-Mn(2)-O(6)$^{\#4}$	158.01(16)
O(1)$^{\#3}$-Mn(1)-O(1)$^{\#1}$	87.91(17)	O(6)$^{\#4}$-Mn(2)-O(7A)	88.5(5)
O(1)-Mn(1)-O(1)$^{\#3}$	158.0(9)	O(6)$^{\#1}$-Mn(2)-O(7A)	88.5(5)
O(1)$^{\#1}$-Mn(1)-O(1)$^{\#2}$	158.0(9)	O(6)$^{\#1}$-Mn(2)-O(7B)	86.0(3)
O(1) -Mn(1)-O(1)$^{\#1}$	87.91(17)	O(6)$^{\#4}$-Mn(2)-O(7B)	86.0(3)
O(1)$^{\#3}$-Mn(1)-O(1)$^{\#2}$	87.91(17)	O(8)-Mn(2)-O(6)$^{\#1}$	100.87(9)
O(1) -Mn(1)-O(1W)	101.0(5)	O(8)-Mn(2)-O(6)$^{\#4}$	100.87(9)
O(1)$^{\#1}$-Mn(1)-O(1W)	101.0(5)	O(8)-Mn(2)-O(7A)	107(2)
O(1)$^{\#2}$-Mn(1)-O(1W)	101.0(5)	O(8)-Mn(2)-O(7B)	102.6(16)
O(1)$^{\#3}$ -Mn(1)-O(1W)	101.0(5)		

Symmetry code: $^{\#1}$ -y+1,x,z; $^{\#2}$ y,-x+1,z; $^{\#3}$ -x+1,-y+1,z; $^{\#5}$ -y+1,x,-z+1

Table S5. Hydrogen bonds for compound **1** (Å and °).

D-H...A	d(D-H)	d(H...A)	d(D...A)	<(DHA)
C(2)-H(2)...O(6)$^{\#10}$	0.95	2.75	3.37(2)	123.4
C(2)-H(2)...O(8)$^{\#11}$	0.95	2.45	3.382(13)	166.2

Symmetry code: $^{\#10}$ -x+3/2,-y+3/2,-z+1/2; $^{\#11}$ -y+3/2,x+1/2,z-1/2

Table S6. Selected bond lengths (Å) and angles (°) for compound **2**.

2			
Cd(1)-O(1)$^{\#8}$	2.201(18)	Cd(2)-O(6A)	1.98(5)
Cd(1)-O(1)$^{\#9}$	2.201(18)	Cd(2)-O(8)$^{\#4}$	1.78(2)
Cd(1)-O(1)	2.201(18)	Cd(2)-O(8)$^{\#1}$	1.78(2)
Cd(1)-O(1)$^{\#10}$	2.201(18)	Cd(2)-O(7)	1.594(18)
Cd(1)-O(1W)	2.47(2)	Cd(2)-O(6B)	1.98(4)

O(6A)-Cd(2)-O(9)$^{\#1}$	107.4(17)	Cd(2)-O(9)$^{\#1}$	2.54(3)
O(1)$^{\#10}$-Cd(1)-O(1)$^{\#9}$	88.77(13)	O(8)$^{\#1}$-Cd(2)-O(6A)	88.7(6)
O(1)$^{\#10}$-Cd(1)-O(1)	88.77(13)	O(8)$^{\#4}$-Cd(2)-O(6A)	88.7(6)
O(1)$^{\#9}$-Cd(1)-O(1)	163.2(9)	O(8)$^{\#4}$-Cd(2)-O(8)$^{\#1}$	152.6(16)
O(1)$^{\#8}$-Cd(1)-O(1)	88.77(13)	O(8)$^{\#1}$-Cd(2)-O(6B)	88.0(6)
O(1)$^{\#10}$-Cd(1)-O(1)$^{\#8}$	163.2(9)	O(8)$^{\#4}$-Cd(2)-O(6B)	88.0(6)
O(1)$^{\#8}$-Cd(1)- O(1)$^{\#9}$	88.77(13)	O(8)$^{\#4}$-Cd(2)-O(9)$^{\#1}$	77.4(8)
O(1)$^{\#8}$-Cd(1)-O(1W)	98.4(4)	O(8)$^{\#1}$-Cd(2)-O(9)$^{\#1}$	77.4(8)
O(1)$^{\#10}$-Cd(1)-O(1W)	98.4(4)	O(7)-Cd(2)-O(6A)	97(2)
O(1)$^{\#9}$-Cd(1)-O(1W)	98.4(4)	O(7)-Cd(2)-O(8)$^{\#4}$	103.7(8)
O(1)-Cd(1)-O(1W)	98.4(4)	O(7)-Cd(2)-O(8)$^{\#1}$	103.7(8)
O(7)-Cd(2)-O(9)$^{\#1}$	156.0(16)	O(7)-Cd(2)-O(6B)	97(2)
O(6B)-Cd(2)-O(9)$^{\#1}$	58.6(17)		

Symmetry code: $^{\#1}$ -y+1,x-1,z ; $^{\#4}$ -y+1,x-1,-z+2; $^{\#8}$ -y+1,x,z; $^{\#9}$ -x+1,-y+1,z; $^{\#10}$ y,-x+1,z

Table S7. Hydrogen bonds for compound **2** (Å and °).

D-H...A	d(D-H)	d(H...A)	d(D...A)	<(DHA)
C(2)-H(2)...O(7)	0.95	2.45	3.39(2)	170.3

Table S8. Selected bond lengths (Å) and angles (°) for compound **3**.

3			
Ni(1)-O(1)$^{\#3}$	1.991(14)	Ni(2)-O(5)	1.799(10)
Ni(1)-O(1)$^{\#1}$	1.991(14)	Ni(2)-O(5)$^{\#6}$	1.799(10)
Ni(1)-O(1)	1.991(14)	Ni(2)-O(9)	1.85(2)
Ni(1)-O(1)$^{\#2}$	1.991(14)	Ni(2)-O(6)	1.846(17)
Ni(1)-O(1W)	2.307(18)	Ni(2)-O(10)	1.659(3)
O(1)$^{\#2}$-Ni(1)-O(1)$^{\#1}$	88.49(13)	O(5) -Ni(2)-O(5) $^{\#6}$	154.8(8)
O(1) $^{\#2}$-Ni(1)-O(1)$^{\#3}$	88.49(13)	O(5)-Ni(2)-O(9)	87.9(4)
O(1)$^{\#3}$-Ni(1)-O(1)$^{\#1}$	161.3(8)	O(5)$^{\#6}$-Ni(2)-O(9)	87.9(4)
O(1)-Ni(1)-O(1)$^{\#2}$	161.38(8)	O(5) -Ni(2)-O(6)	86.3(4)

O(1) -Ni(1)-O(1)$^{\#3}$	88.49(13)	O(5) $^{\#6}$-Ni(2)-O(6)	86.3(4)
O(1)-Ni(1)-O(1)$^{\#1}$	88.49(13)	O(10)-Ni(2)-O(5)$^{\#6}$	102.6(4)
O(1)$^{\#1}$-Ni(1)-O(1W)	99.4(4)	O(10)-Ni(2)-O(5)	102.6(4)
O(1)-Ni(1)-O(1W)	99.4(4)	O(10)-Ni(2)-O(9)	103.7(13)
O(1)$^{\#3}$-Ni(1)-O(1W)	99.4(4)	O(10)-Ni(2)-O(6)	103.2(11)
O(1)$^{\#2}$-Ni(1)-O(1W)	99.4(4)		

Symmetry code: $^{\#1}$ -y+1,x,z； $^{\#2}$ -x+1,-y+1,z； $^{\#3}$ y,-x+1,z； $^{\#6}$ x,y,-z+1

Table S9. Hydrogen bonds for compound **3** (Å and °).

D-H...A	d(D-H)	d(H...A)	d(D...A)	<(DHA)
C(2)-H(2)...O(10)$^{\#10}$	0.93	2.26	3.154(14)	162.2

Symmetry code: $^{\#10}$ y+1/2,-x+3/2,z-1/2

References

1. G.M. Sheldrick, SHELXS−2018, Programs for X−ray Crystal Structure Solution; University of Göttingen: Göttingen, Germany, 2018.
2. L.J. Farrugia, WINGX: A Windows Program for Crystal Structure Analysis; University of Glasgow: Glasgow, UK, 1988.
3. G.M. Sheldrick, SHELXTL−2018, Programs for X−ray Crystal Structure Refinement; University of Göttingen: Göttingen, Germany, 2018.
4. Y. Li, Y. Wu, H. Jiang and H. Wang, In situ stable growth of Bi_2WO_6 on natural hematite for efficient antibiotic wastewater purification by photocatalytic activation of peroxymonosulfate, *Chem. Eng. J.*, 2022, **446**, 136704.
5. C. Athanasekou, G. E. Romanos, S. K. Papageorgiou, G. K. Manolis, F.

Katsaros and P. Falaras, Photocatalytic degradation of hexavalent chromium emerging contaminant via advanced titanium dioxide nanostructures, *Chem. Eng. J.*, 2017, **318**, 171–180.

6. Y. Zhang, H. Li, X. Zhang, H. Zhang, W. Zhang, H. Huang, H. Ou and Y. Zhang, Enhanced adsorption and photocatalytic Cr(VI) reduction and sterilization of defective MoS_2/PVP, *J. Colloid Interface Sci.*, 2023, **630**, 742−753.
7. R. Fatima and J. O. Kim,, Photocatalytic reduction of chromium by titanium metal organic frameworks in the presence of low−molecular−weight organic acids under UV and visible light, *J. Environ. Chem. Eng.*, 2022, **10(6)**, 108796.
8. I. Ibrahim, A. Kaltzoglou, C. Athanasekou, F. Katsaros, E. Devlin, A. G. Kontos, N. Ioannidis, M. Perraki, P. Tsakiridis, L. Sygellou, M. Antoniadou and P. Falaras, Magnetically separable TiO_2/$CoFe_2O_4$/Ag nanocomposites for the photocatalytic reduction of hexavalent chromium pollutant under UV and artificial solar light, *Chem. Eng. J.*, 2020, **381**, 122730.
9. M. Velumani and J. Jeyadharmarajan, Conversion of novel tannery sludge−derived biochar/TiO_2 nanocomposite for efficient removal of Cr (VI) under UV light: photocatalytic performance and mechanism insight, *Environ. Sci. Pollut. Res.*, 2023, **30(10)**, 28173−28191.
10. N. Ahmad, C.-F. J. Kuo and M. Mustaqeem, Synthesis of novel $CuNb_2O_6$/g−C_3N_4 binary photocatalyst towards efficient visible light reduction of Cr (VI) and dyes degradation for environmental remediation, *Chemosphere*,

2022, **298**, 134153.

11. F. Yuan, Z. Sun, C. Li, Y. Tan, X. Zhang and S. Zheng, Multi−component design and in−situ synthesis of visible−light−driven SnO_2/g−C_3N_4/diatomite composite for high−efficient photoreduction of Cr(VI) with the aid of citric acid, *J. Hazard. Mater.*, 2020, **396**, 122694.
12. R. Wang, C. V. Reddy, B. Talluri, R. R. Kakarla, R. R. Zairov, J. Shim and T. M. Aminabhavi, Cobalt−doped V_2O_5 hexagonal nanosheets for superior photocatalytic toxic pollutants degradation, Cr (VI) reduction, and photoelectrochemical water oxidation performance, *Environ. Res.*, 2023, **217**, 114923.
13. C. Hu, B. Yu, Z. Zhu, J. Zheng, W. Wang and B. Liu, Construction of novel S−scheme $LaFeO_3$/g−C_3N_4 composite with efficient photocatalytic capacity for dye degradation and Cr(VI) reduction, *Colloid Surf. A−Physicochem. Eng. Asp.*, 2023, **664**, 131189.
14. Q. Wang, L. Wang, S. Zheng, M. Tan, L. Yang, Y. Fu, Q. Li, H. Du and G. Yang, The strong interaction and confinement effect of Ag@NH_2−MIL−88B for improving the conversion and durability of photocatalytic Cr(VI) reduction in the presence of a hole scavenger, *J. Hazard. Mater.*, 2023, **451**, 131149.
15. Y. Gao, Y. Huang, M. Bao, X. Zhang, X. Zhou, L. Liu, Z. Zhang, L. Zeng and J. Ke, Ti−doped Zr−UiO−66−NH_2 boosting charge transfer for enhancing the synergistic removal of Cr (VI) and TC−HCl in wastewater, *Process Saf. Environ. Protect.*, 2023, **172**, 857−868.

16. Y. Gong, Z. Xu, J. Zhong, D. Ren, D. Ma, M. Li and S. Huang, Construction of S−scheme CdS/g−C_3N_4 heterojunctions with enhanced photocatalytic H_2 evolution and Cr(VI) reduction performance, *J. Phys. Chem. Solids*, 2023, **180**, 111421.
17. Y. Zhang, P. Tan, L. Yang, S. Zhang, B. Zhou, X. Zhang, H. Huang and J. Pan, Mannitol−assisted Fe−O clusters@ZIF−L for Cr(VI) photocatalytic reduction under neutral conditions inspired by Fe−based MOFs photocatalysts, *Sep. Purif. Technol.*, 2023, **320**, 124174.
18. Y. Liu, F. Gao, S. Liu, H. Liu, M. Fang and X. Tan, Visible and infrared light photocatalysis of Cr(VI) by CdTe nanoparticles, *Appl. Surf. Sci.*, 2023, **615**, 156399.
19. S. Li, M. Cai, C. Wang, Y. Liu, N. Li, P. Zhang and X. Li, Rationally designed Ta_3N_5/BiOCl S−scheme heterojunction with oxygen vacancies for elimination of tetracycline antibiotic and Cr(VI): Performance, toxicity evaluation and mechanism insight, *J. Mater. Sci. Technol.*, 2022, **123**, 177−190.
20. X. Gao, B. Li and S. Jian, Step−scheme CeO_2/$CaIn_2S_4$ heterostructured photocatalysts for efficient reduction of Cr(VI) under visible light, *Colloid Surf. A−Physicochem. Eng. Asp.*, 2022, **648**, 129168.
21. Q. Li, Z.-Q. Wu, D. Li, T.-H. Liu, H.-y. Yin, X.-B. Cai, W. Zhu, Z.-L. Fan and R.-Z. Li, A Tb^{3+}−anchored Zr(IV)−bipyridine MOF to promote photo−induced electron transfer and simultaneously enhance photoluminescence ability and photocatalytic reduction efficiency towards $Cr_2O_7^{2-}$, *J. Mater. Chem. A*, 2023,

11(6), 2957−2968.

22. H. Kaur, S. Sinha, V. Krishnan and R. R. Koner, Photocatalytic Reduction and Recognition of Cr(VI): New Zn(II)−Based Metal−Organic Framework as Catalytic Surface, *Ind. Eng. Chem. Res.*, 2020, **59(18)**, 8538−8550.
23. L. Wang, T. Zeng, G. Liao, Q. Cheng and Z. Pan, Syntheses, structures and catalytic mechanisms of three new MOFs for aqueous Cr(VI) reduction and dye degradation under UV light, *Polyhedron*, 2019, **157**, 152−162.
24. Z. Pan, C.-C. Cai, T.-T. Li, C.-W. Lou, J.-H. Lin and H.-T. Ren, Multipath collaboration mechanisms involved in the photocatalytic reduction of Cr(VI) by $FeC_2O_4/Bi_{2.15}WO_6$, *J. Photochem. Photobiol. A−Chem.*, 2023, **445**, 115099.
25. H.-T. Ren, Z. Pan, W.-B. Cao, T.-T. Li, C.-W. Lou, J.-H. Lin and X. Han, Facile synthesis of Ti_3C_2 MXene−modified $Bi_{2.15}WO_6$ nanosheets with enhanced reactivity for photocatalytic reduction of Cr(VI), *Adv. Powder Technol.*, 2022, **33(9)**, 103722.
26. R. Yang, S. Zhong, L. Zhang and B. Liu, $PW_{12}/CN@Bi_2WO_6$ composite photocatalyst prepared based on organic−inorganic hybrid system for removing pollutants in water, *Sep. Purif. Technol.*, 2020, **235**, 116270.
27. ZZ. Lv, H. Zhou, H. Liu, B. Liu, M. Liang and H. Guo, Controlled assemble of oxygen vacant $CeO_2@Bi_2WO_6$ hollow magnetic microcapsule heterostructures for visible−light photocatalytic activity, *Chem. Eng. J.*, 2017, **330**, 1297−1305.
28. D. Y. Peng, H.-Y. Zeng, J. Xiong, F. Y. Liu, L. H. Wang, S. Xu, Z.-L. Yang and S.-G. Liu, Tuning oxygen vacancy in Bi_2WO_6 by heteroatom doping for

enhanced photooxidation−reduction properties, *J. Colloid Interface Sci.*, 2023, **629**, 133−146.

29. J. Dong, J. Hu, A. Liu, J. He, Q. Huang, Y. Zeng, W. Gao, Z. Yang, Y. Zhang, Y. Zhou and Z. Zou Simple fabrication of Z−scheme $MgIn_2S_4/Bi_2WO_6$ hierarchical heterostructures for enhancing photocatalytic reduction of Cr(VI), *Catal. Sci. Technol.*, 2021, **11(18)**, 6271.
30. S. Li, M. Cai, Y. Liu, J. Zhang, C. Wang, S. Zang, Y. Li, P. Zhang and X. Li, In situ construction of a C_3N_5 nanosheet/Bi_2WO_6 nanodot S−scheme heterojunction with enhanced structural defects for the efficient photocatalytic removal of tetracycline and Cr(VI), *Inorg. Chem. Front.*, 2022, **9(11)**, 2479−2497.
31. G. Wu, Q. Liu, J. Wang, S. Xia, X. Huang, J. Han and W. Xing, Construction of hierarchical $Bi_2WO_6/ZnIn_2S_4$ heterojunction for boosting photocatalytic performance in degradation of organic compounds and reduction of hexavalent chromium, *Colloid Surf. A−Physicochem. Eng. Asp.*, 2022, **653**, 130048.
32. S. Li, M. Cai, Y. Liu, C. Wang, K. Lv and X. Chen, S−Scheme photocatalyst TaON/Bi_2WO_6 nanofibers with oxygen vacancies for efficient abatement of antibiotics and Cr(VI): Intermediate eco−toxicity analysis and mechanistic insights, *Chin. J. Catal.*, 2022, **43(10)**, 2652−2664.